Chapter 3

Impregnated Cu(II) onto a pyridine-based porous organic polymer as robust heterogeneous catalyst for nitroarene reduction

3.1 Abstract

This chapter describes the excellent heterogeneous catalytic activity exhibited by Cu(II) catalyst incorporated onto a pyridine based porous organic polymer for nitroarene reduction. Results demonstrated its improved catalytic performances over those reported using expensive and precious metals (like Au and Pd) on immobilized organic porous materials. The confinement effect of polymeric network over immobilized Cu(II) has been investigated by EDX elemental mapping which shows uniform distribution of Cu providing larger active sites for catalysis. The oxidation states behavior of copper onto the POP was monitored by XPS study. The π-electrons rich pyridine based amide functionalized POP scaffold facilitates electron transfer to the finely dispersed Cu sites and accountable for the efficient and effective catalytic activity tested in nitroarene reduction supported by improved stability of the catalyst.

3.2 Introduction

Growing industries and agricultural factories in order to meet the human needs expose various pollutants along with water to the environment. Such exposure creates a serious threat to the life of plants, animals and even human beings. One amongst the toxic contaminants is 4-nitrophenol (4NP), a widely used harmful chemical especially in agricultural industries. Detoxification of 4NP by conventional water treatment technique is of rising concern owing to its high chemical stability and resistivity towards microbial degradation. In this context, reduction of 4NP to corresponding 4-aminophenol (4AP), an important precursor compound in pharmaceutical and plastic industries is graded as wise alternate. But under ideal conditions in absence of a catalyst the reduction of 4NP and/or nitroarenes does not proceed. Whereas it can easily be reduce to aminophenol in presence of a metal catalyst. Conventional method for the reduction of nitro group is with iron/acid but the process is not regarded as environmentally benign.

During the past few decades 4NP reduction reactions witnessed the involvement of precious noble metals (Au, Pt, Pd, Rh, Ru, etc.) based heterogeneous catalysts [1,2].

Further reports demonstrating the utility of bimetallic materials as good candidate in performing heterogeneous catalysis of organic reactions are also available [3,4]. For example, Kim et al. synthesized Pd–Pt bimetallic nanoparticles supported by carbon nanotube [5]. It reveals excellent and efficient catalytic activity through synergistic effect towards the reduction of 4NP along with chemoselectivity in reduction of other nitroarenes. Immobilized Au nanoparticles rooted in covalently mediated self-assembled polymeric membrane of nanocomposites have further established its effectiveness in such reductions [6]. Use of porous materials with tailored properties such as pore radius, surface area, pore volume, etc. are recent concerns as catalyst carrier in organic transformation reactions [7,8].

The nitrophenol reduction has been considered as one of the extremely popular reaction to essay catalytic activity. A predesigned conjugated microporous polymer (CMP) with potent metal binding sites has been synthesized to afford Ag^0@CMP capturing Ag^+ ion [9]. The Ag(0) loaded CMP had eventually explored as nanocatalyst with significant performance for reduction of 4NP with $NaBH_4$. Huang et al. illustrated the catalytic activity of Rh nanoparticles incorporated over porous ionic copolymer (PICP) in the selective reduction of functionalized nitroarenes leaving the functional groups unaffected [10]. Liu et al. synthesized a carbon porous material (CPM) that acts as a support matrix for impregnation of Pd that shows better catalytic efficiency in reduction of 4NP [11]. In addition, a fine hollow Ag nanocage with controlled size had been demonstrated revealing catalytic behavior in nitrophenol reduction [12]. Banerjee and his group lately employed the imine linked covalent organic framework (COF) loaded with gold (Au) for the reduction of 4NP [13]. The metal organic frameworks (MOFs) as a support for encapsulating palladium (Pd) nanoparticles for carrying out the nitrophenol reduction was also reported [14].

In recent years, porous polymer or silica has been accomplished as an excellent catalytic scaffold for incorporation of metals to improve its activity, especially in performing heterogeneous catalysis. Therefore the way of doing catalytic reactions has now oriented towards the preparation of heterogeneous supported catalysts. Needless to mention that such supported catalysts have continued to show thermal and chemical stability during the reaction process. In addition, presence of suitable functional groups, high surface area and porosity in the structural framework of the support matrix stimulate the catalytic

process through intermolecular interactions. Built with functional moieties, these porous materials can be nucleated heterogeneously with metals to act as heterogeneous catalyst. Porous carbon materials (PCM) was initially tested as support matrix for transformation reactions and emerged as popular support catalyst and opened a new avenue toward potent applications of PCM in catalysis [15,16]. The heteroatom enriched PCM garnered wide outstanding applications with remarkable performance and stability in this field. A phosphorus doped carbon based porous material also known as 'green catalyst' was used as metal free heterogeneous catalyst in selective oxidation of benzyl alcohols in air [17]. Metal free oxidation reaction has also been accomplished by nitrogen doped graphene nanosheets with N serving as an active catalytic center [18]. Boron nitride nanosheets also showed useful applications after the impregnation of active metals. The successful immobilization of Pd nanoparticles in such nanosheets has also been established that shows promising catalytic activity in reduction of nitroarenes facilitated by electron push mechanism aided by B and N of the nanosheet [19].

Porous organic polymers (POPs) and/or covalent organic frameworks (COFs) are a new class of high surface area materials that exhibits excellent support matrix for transition metal incorporation. It thereby accomplished potent applications in photocatalysis and as heterogeneous catalyst [20-25]. The profound catalytic activity of Ru nanoparticles loaded porous network in the biodiesel production from renewable sources has been demonstrated [21]. Meanwhile the role of amide functionality of a porous polymer framework in gas adsorption and catalytic activity in selective oxidation reactions is demonstrated in Chapter 2 [26]. Understanding the significance of POPs and/or COFs in gas adsorption, sensing, proton conduction, gas storage and separation, catalysis, drug delivery etc., various functional groups into the porous network were attempted to impregnate to tune chemical properties [26,27-29]. The functional groups are nucleated heterogeneously with the metals or metals to load onto the pore and/or surface to act as heterogeneous catalyst [30-32]. The catalytic activity of an imine based 2D-COF (COF-LZU1) for Suzuki Miyaura coupling reaction was explored by loading Pd ion into the cavities of porous framework [33]. Presence of nitrogen heteroatom in COF-LZU1 remains advantageous for better catalytic activity due to stabilization of the encapsulated materials. Imine linked POPs have been described commonly in the literature; especially these materials were used as the scaffold for carrying metal ions and perform the catalytic activity [34-37]. For example, a hydroxyl functionalized triazine ring based

framework with imine linkage docked by Cu(II) has been reported as an excellent catalyst for the selective oxidation of olefins [38]. Triazine based organic frameworks are also illustrated pretending as catalytic bed in performing the cycloaddition reaction of CO_2 and glycerol oxidation respectively [39]. The COF and/or POP supported catalysts in various organic reactions such as Mizoroki-Heck coupling [40], Chan Lam coupling [34], Knoevenagel condensation [35], cascade [36], Diels Alder reactions [41] etc. have also been reported.

In view of the importance of nitrogen centers with lone pair electrons and amide functionality, a new organic porous polymer material has been synthesized. The polymer scaffold was employed as support matrix in loading cheaper metals like copper. The catalytic influence of the copper loaded polymer is successfully tested for the widely popular nitroarene reduction reaction and results are demonstrated in this chapter [42]. The Cu loaded porous polymer displays excellent catalytic behavior for 4NP reduction to 4AP in shortest reaction time with improved yield percentage (%) compared to those reported using precious and expensive metal supported POPs and /or COFs.

3.3 Results and Discussion

3.3.1 Synthesis of pyridine based porous polymer

A new pyridine based two dimensional POP is designed and synthesized by Schiff-base chemistry from 2,4,6-tris(4-aminophenyl)pyridine (TAPPy) as building block and 1,3,5–benzenetricarbonyl trichloride (BzCl) as organic linker (Scheme 3.1).

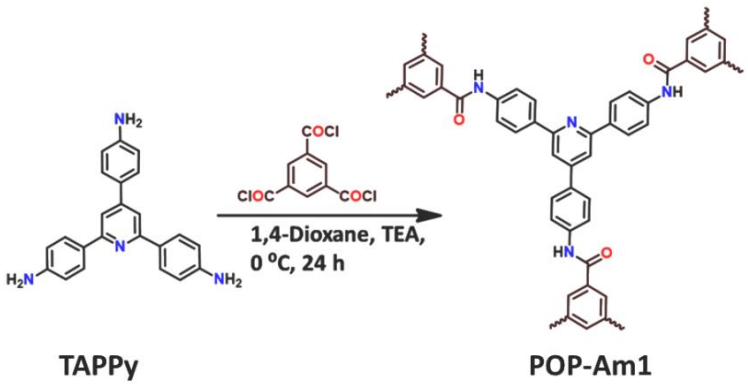

Scheme 3.1 Schematic representation of POP-Am1 synthesis from 2,4,6-tris(4-aminophenyl)pyridine (TAPPy) and 1,3,5-benzenetricarbonyl trichloride (BzCl).

The synthesized polymer (hereafter POP-Am1) is characterized using FT-IR, solid state NMR, PXRD, TGA, SEM, and TEM studies.

3.3.2 Characterization of POP-Am1

The formation of amide C=O in POP-Am1 is evidenced by the disappearance of strong and sharp C=O stretching frequency of carbonyl of BzCl at 1753 cm^{-1} and appearance of stretching band at 1659 cm^{-1} responsible for amide C=O in the IR spectrum of POP-Am1 (Figure 3.1a). Also the peak at stretching frequency 3445 cm^{-1} and 3358 cm^{-1} of N−H stretching vibration of TAPPy disappears and a new stretching for the carboxamide N−H appears at 3230 cm^{-1}.

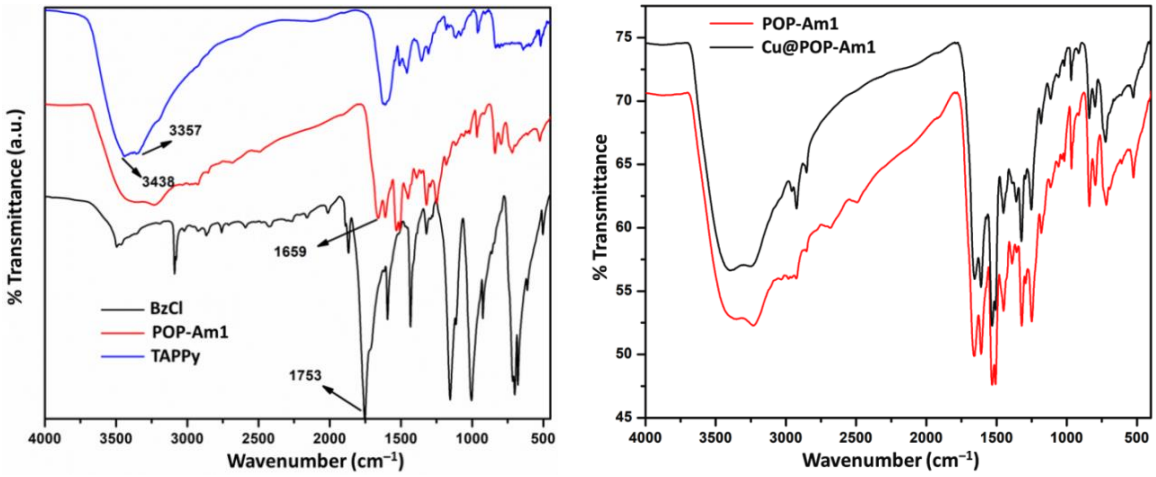

Figure 3.1 Comparison of FT-IR spectra of POP-Am1 and the building units signify the occurrence of amide functionality in POP-Am1 (a) and FT-IR spectra comparison indicates retention of structural integration of POP-Am1 upon impregnation of Cu(II) to afford Cu@POP-Am1.

The formation of -CONH- linkage was further confirmed by ^{13}C CP-MAS solid state NMR (ssNMR) spectroscopy. The chemical shifts of carbon in ^{13}C ssNMR spectrum of POP-Am1 (Figure 3.2) appears at 9, 47, 119, 122, 124, 127, 131, 133, 138, 150, 151 and 166 ppm of which peak at 166 ppm for -CONH- carbon further confirms the formation of POP-Am1. A sharp peak at 9 and 47 ppm in the spectrum reveals the inclusion of triethylammonium chloride salt into the pores of the polymer. The identical chemical shift value for triethylammonium chloride salt was reported in the literature and compared for subtraction [43].

The inclusion of guest molecules, i.e. triethylammonium chloride in pores of POP-Am1 is further evidenced by recording the TGA plot and PXRD pattern. Significant amount (~20 %) of weight loss in the temperature range of 140 to 260 °C is revealed in the TGA plot (Figure 3.3a). This indicates the inclusion of guest molecules in POP-Am1. Moreover, the firm evidence about the guest molecules to be triethylammonium chloride was witnessed from the PXRD pattern (Figure 3.4a). The pattern shows several sharp peaks at 2θ = 12, 17, 21, 24, 25 and 27. They corresponds to the crystalline triethylammonium chloride (Figure 3.4a inset, retrieved from literature) already incorporated in the cavities during the synthesis and isolation process of POP-Am1 [43]. The guest free pure POP-Am1 was isolated upon heating it at 200 °C for 1 h and is assured by recording PXRD pattern (Figure 3.4b). The diffraction pattern of purified POP-Am1 renders the formation of amorphous porous material.

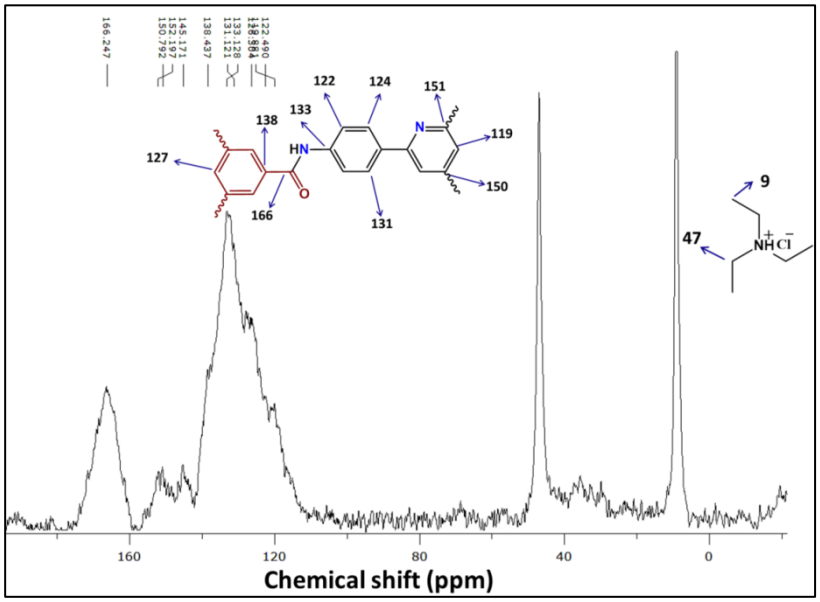

Figure 3.2 ^{13}C cross-polarization magic angle spinning (^{13}C CP-MAS) ssNMR spectroscopy shows chemical shift environments of various carbon centers of POP-Am1.

The nitrogen adsorption and desorption isotherm at 77 K (Figure 3.5a) exposes the permanent porosity and rigidity of POP-Am1. The pore size distribution curve is depicted in Figure 3.5b. The lack in hysteresis of the isotherm signifies the reversible nature of nitrogen adsorption indicating identical adsorption-desorption mechanism. The Brunauer–Emmet–Teller (BET) surface area of POP-Am1 is found to be 27 m^2g^{-1} and an average pore diameter of 29.24 Å affirms the polymer to be microporous in nature. Even though the majority of porous materials exhibit high surface area, the existence of porous

materials with lower surface area cannot be denied. Porous polymer witnessing with the lower value of surface area (20-32 m^2g^{-1}) having identical adsorption isotherm has recently been reported [44]. The FE-SEM image elucidates the surface morphology comprising of spherical shape with diameter 1 μm (Figure 3.6a,b). Whereas the layered structure of POP-Am1 is revealed by TEM image (Figure 3.6c,d).

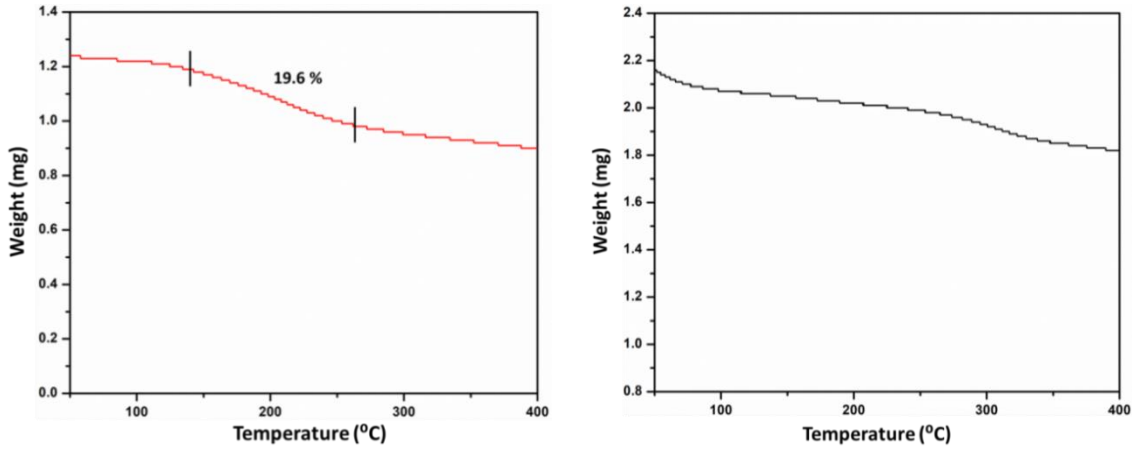

(a) (b)

Figure 3.3 TGA plot of (a) as synthesized POP-Am1 indicates inclusion of guests into the pores and (b) confirms thermal stability of Cu@POP-Am1 up to 400 ºC.

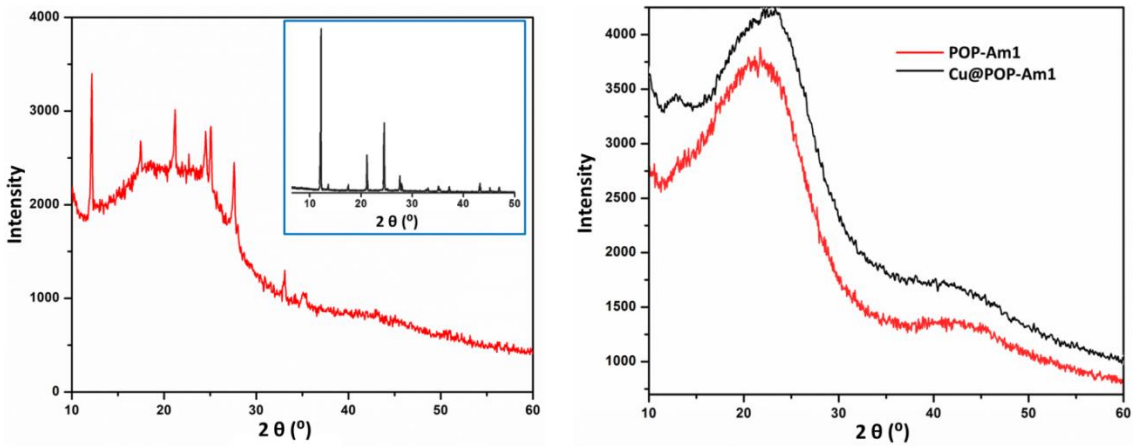

(a) (b)

Figure 3.4 (a) Sharp crystalline peak in PXRD pattern of as synthesized POP-Am1 indicates the trapping of triethylammonium chloride salt in the cavities (inset: PXRD pattern of triethylammonium chloride salt retrieved from literature) and (b) PXRD pattern of activated POP-Am1 and Cu@POP-Am1 signifying the intact structure of bare POP-Am1 upon metal impregnation.

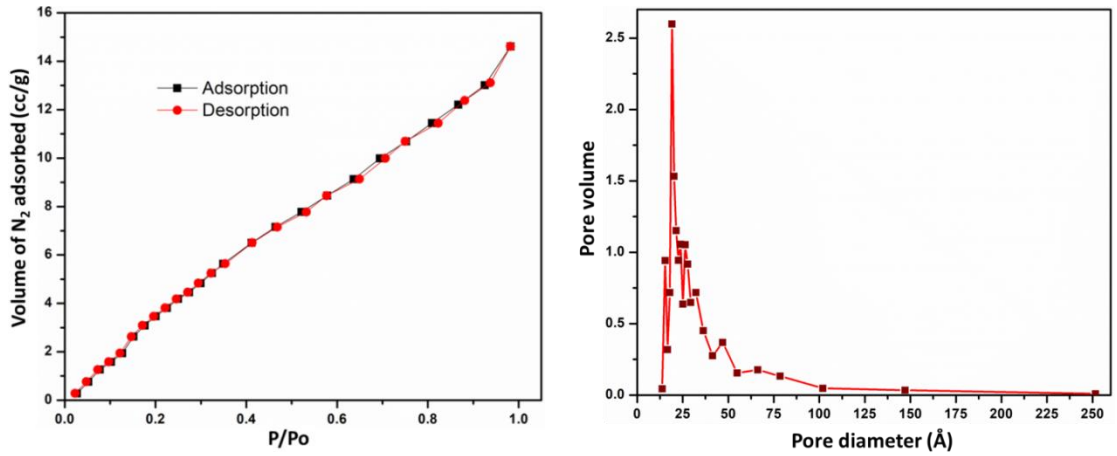

(a) (b)

Figure 3.5 The reversible nitrogen adsorption-desorption isotherm recorded at 77 K (a) and the pore size distribution curve displaying microporous nature (b) of POP-Am1.

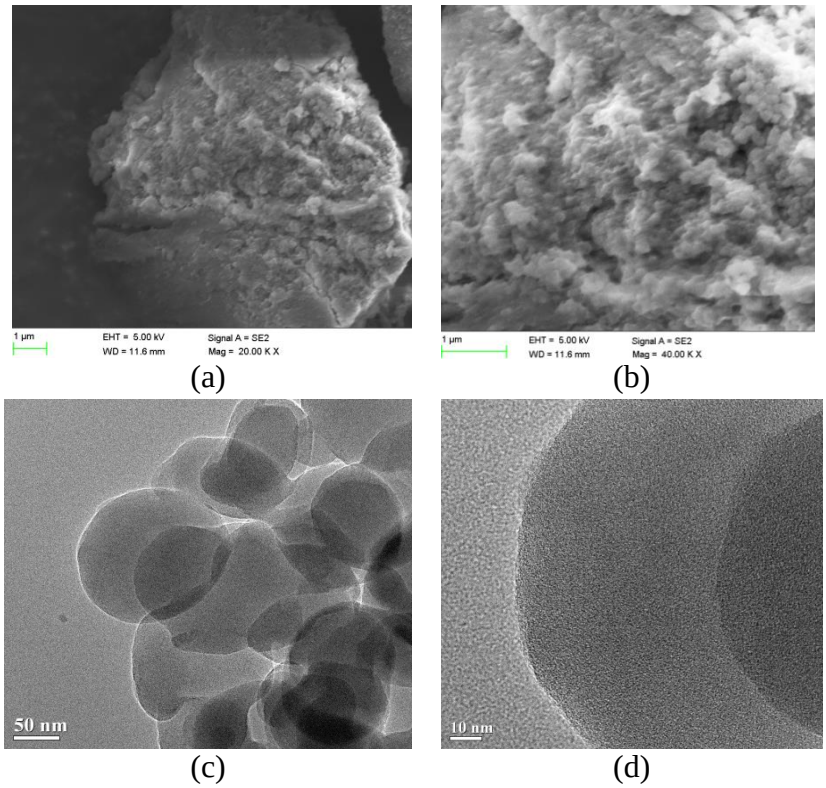

(a) (b)

(c) (d)

Figure 3.6 FE-SEM images (a,b) and HR-TEM images (c,d) of activated POP-Am1.

3.3.3 Synthesis and characterization of Cu@POP-Am1

The network solids having nitrogen heteroatom remain advantageous for better performance of catalytic activity and a versatile moiety to stabilize the encapsulated and/or loaded metals. Indeed, the nitrogen containing ligand in coordination chemistry is well demonstrated to coordinate metal ions. In this context, the availability of lone pair electrons on pyridine N and on the O of amide group in the architecture of POP-Am1

provides opportunity to coordinate with metals. Thus, the characterized POP-Am1 is considered to act as heterogeneous catalyst carrier and loaded with Cu(II) by impregnation method to give metal immobilized onto POP-Am1 (hereafter Cu@POP-Am1, Scheme 3.2).

The desired copper loaded POP-Am1 (Cu@POP-Am1) was characterized using FT-IR, TGA, PXRD, EDS, AAS, ICP, TEM and XPS analytical techniques. FT-IR analysis disclosed Cu@POP-Am1 to be nearly identical in the structural integrity to POP-Am1 (Figure 3.1b). The identical IR spectra with resemblance in stretching frequencies of amide C=O at 1610 cm^{-1} and for N–H at 3230 cm^{-1} specifies preservation of structure of POP-Am1 in Cu@POP-Am1.

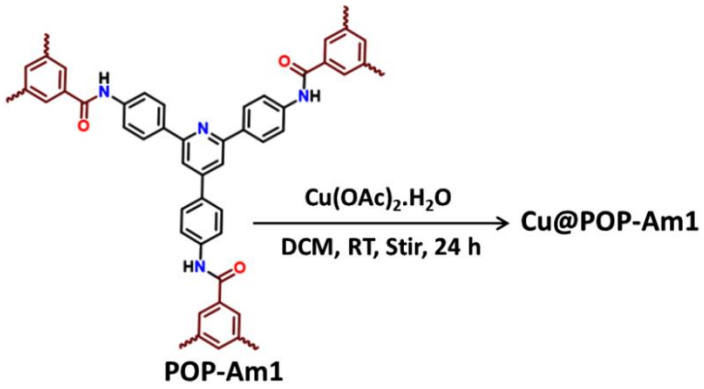

Scheme 3.2 Synthetic representation of Cu@POP-Am1 from POP-Am1.

The intact structural integrity of POP-Am1 upon metal incorporation could be gathered by comparing the PXRD patterns of Cu@POP-Am1 with that of bare POP-Am1. Identical patterns support no structural dissimilarity of POP-Am1 upon loading of copper metal (Figure 3.4b). The Cu ions are practically mobilized onto the POP-Am1 and intact non-crystalline behavior is affirmed by PXRD diffraction pattern with no sharp peak corresponds to the metal salt.

Further information on behavioral change of POP-Am1, if any, upon impregnation of Cu onto it is procured from electron microscopic imaging. The TEM image of Cu@POP-Am1 in Figure 3.7 displays the preserved layer sheet of POP-Am1. The Cu ions are distributed uniformly onto the pores of POP-Am1 evidenced from recording the elemental mapping (Figure 3.8).

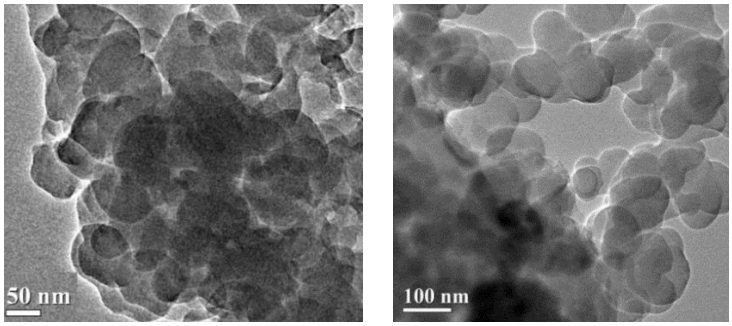

(a) (b)

Figure 3.7 TEM images of Cu@POP-Am1 collected after immobilization of copper acetate onto POP-Am1.

Further support for the existence of Cu is provided by recording the EDS spectrum (Figure 3.9). From SEM-EDS investigation the amount of Cu loaded was calculated to be ~0.9 % by weight. Approximately equivalent weight percentages were detected in AAS (~1.0 %) and ICP (~1.0 %) spectroscopic studies. In addition the stability of the Cu loaded material was also measured by plotting TGA curve. It validates the thermal stability of Cu@POP-Am1 (Figure 3.3b) up to 400 °C as no observable change was detected in the plot.

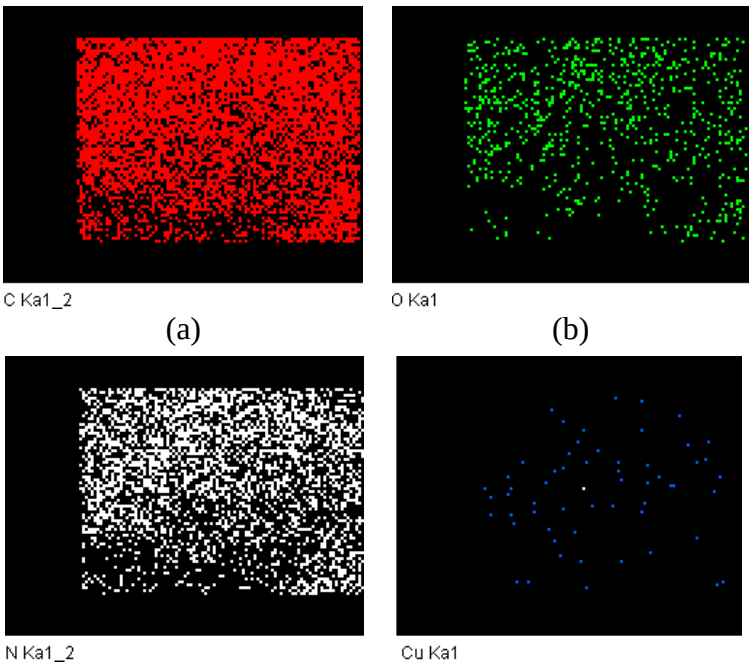

(a) (b)

(c) (d)

Figure 3.8 Elemental mapping showing dispersion of C (a), oxygen (b), nitrogen (c) and homogeneous fine dispersion of Cu (d) in Cu@POP-Am1.

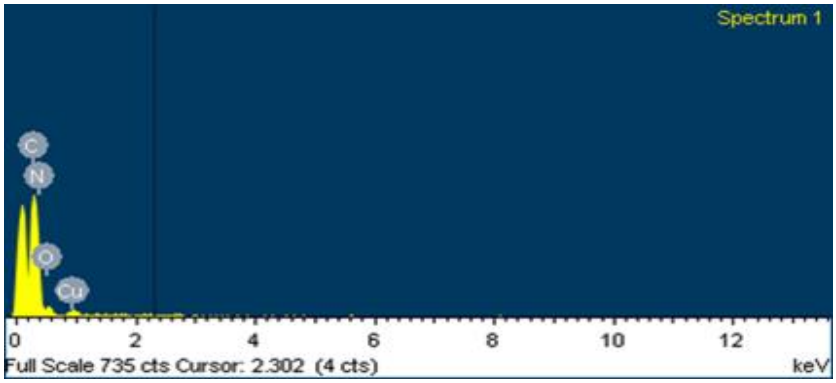

Figure 3.9 EDS spectrum displaying the presence of Cu in Cu@POP-Am1.

3.3.4 Kinetics Study of catalytic reduction of nitroarenes by Cu@POP-Am1

The characterized Cu@POP-Am1 was set to investigate its catalytic activity towards the reduction of nitroarene to the corresponding aminoarene in presence of $NaBH_4$ as a reducing agent. As drawn the attention of nitroarene reduction reaction extensive research in 4-nitrophenol reduction has been perceived and is still persists. In large, literature methods uncover the use of precious metals such as Au, Pt, Pd as catalysts on support matrix. But these are associated with either longer reaction time, or lack of recyclability of the catalysts. Excitingly the reduction was catalyzed at much faster rate using Cu@POP-Am1 than the Au and Pd loaded porous polymers. Employing UV-vis absorption spectroscopy the catalytic activity of Cu@POP-Am1 for the progress of reaction is monitored. In the process, 6 mg of Cu@POP-Am1 was dissolved in 15 ml of water and added 13 mg of $NaBH_4$ and the mixture was left stirred for 3-4 minutes at room temperature. To this added 0.5 mg 4NP in 1 ml of aqueous solution and the reaction progress towards the formation of 4AP was monitored (Figure 3.10a).

Initially, the absorption maximum of faded yellow solution of 4NP appears at wavelength 313 nm. Upon addition of $NaBH_4$ the absorption is shifted to 400 nm with intense yellow coloration owing to the formation of sodium phenolate ion. Change in coloration is expected from $n \rightarrow \pi^*$ transition of the nitro group. As expected the reduction of nitro group to amino does not occurs substantially until the reaction is accelerated by the suitable catalyst. As reaction progress, the absorbance band at 400 nm starts diminishing and a new weak absorption peak at 298 nm starts appearing (Figure 3.10a). In the meantime the yellow color of the solution subsequently fades away and turns into colorless. The decrease in wavelength of absorption from 400 nm to 298 nm is

associated due to change in the electronic transition from n→π* to n→σ* and the formation of 4AP is attributed. The gradual reduction of 4-nitrophenolate affording 4-aminophenol is clearly visible in Figure 3.10a reflecting the role of Cu@POP-Am1 in catalyzing the reduction of 4-nitrophenolate to corresponding aminophenol. The conversion kinetics of the reaction is depicted in the inset of Figure 3.10b and it represents a pseudo first order reaction kinetics. The rate constant is calculated to be, k = 2.16×10^{-2} s^{-1} (Figure 3.10b, inset). It is determined from the slope obtained by plotting $\ln[A_t/A_0]$ vs time, where "A_t" represents the absorbance of phenolate ion at time "t" and "A_0" being the initial absorbance.

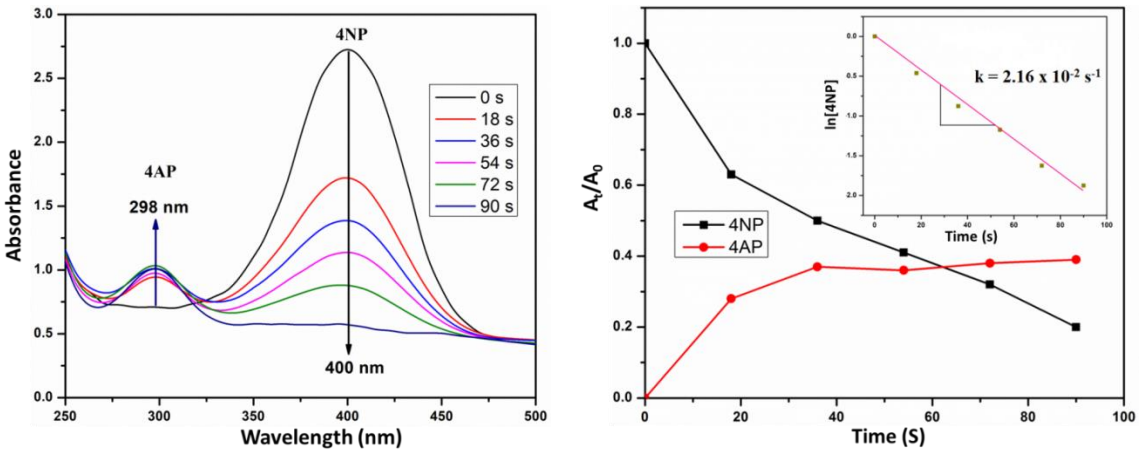

Figure 3.10 UV-visible absorption spectra depicting the reduction of 4NP to 4AP upon using reduced Cu@POP-Am1 (a) and the concentration change of 4NP and 4AP with respect to time as the reaction progress (b).

Usually the surface catalyzed reactions involving two reactants occur in two different ways. Firstly, there exists collision of one molecule on the surface of the reactant molecule that is already being adsorbed on the catalyst surface via Eley-Rideal mechanism which is a second order reaction kinetics [1]. Secondly, the reactant molecules first get adsorbed on the surface and then encounter to give the product via Langmuir-Hinshelwood kinetics [1,45]. In this, the reaction proceeds via 2nd order reaction kinetics. However, a Pseudo first order reaction kinetics is also possible. In present investigation of the nitroarene transformation to aminoarene both the reactant molecule and the reducing agent first get adsorbed on the surface of the porous material and then encounter each other. During the process the surface yielded a reduced product. Since focus is on monitoring the reduction reaction, the effect of stoichiometry of the

reducing agent i.e. $NaBH_4$ is excluded and in little excess amount forces the reaction kinetics to be pseudo first order.

An interesting observation is that the time required for the conversion of 4NP is 10 min when Cu@POP-Am1 is dispersed into the phenolate solution (Figure 3.11a) and the rate constant k changes to 2.50×10^{-3} s^{-1} (Figure 3.11b, inset). The difference in rate of the reaction is due to- (i) Cu@POP-Am1 is immersed in the aqueous solution and reduced adding $NaBH_4$ followed by addition of 4NP solution to the mixture in the previous case, and (ii) in later case, Cu@POP-Am1 is added to the solution mixture already containing 4NP and $NaBH_4$, and reduced in-situ.

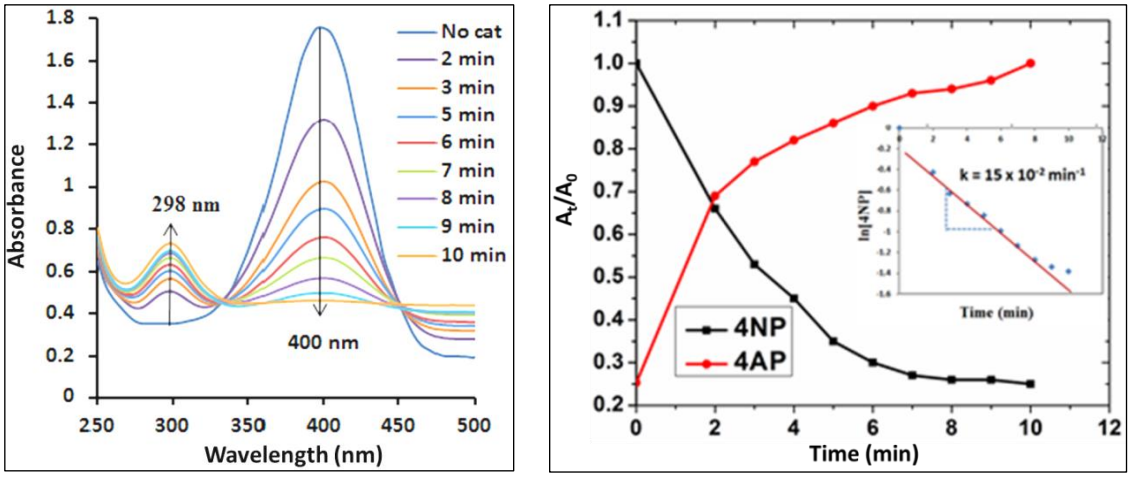

(a) (b)

Figure 3.11 UV-visible spectra of reduction of 4NP with time employing in-situ generated reduced Cu@POP-Am1 using $NaBH_4$ displays longer time for completion of 4NP reduction (a), change in concentration of 4NP and 4AP with respect to time during the progress of reaction (b).

In order to understand the role of other substituents like CH_3O–, CH_3– etc. in lieu of –OH on the reaction kinetics the nitroarenes reduction was carried out with substrates having this substituent's, and evaluated the catalytic behavior of Cu@POP-Am1. In another set of experiment isomeric nitroanilines were viewed to perceive the effect of –NH_2 group on the reaction kinetics. It reveals the reduction of *p*-nitroaniline (*p*-NA) to the corresponding *p*-phenylenediammine (*p*-PD) in presence of Cu@POP-Am1 requires only 36 min (Figure 3.12a). Whereas, *m*-nitroaniline (*m*-NA) takes 55 min (Figure 3.12b) to get reduce and *o*-nitroaniline (*o*-NA) does not reduce at all (Figure 3.13).

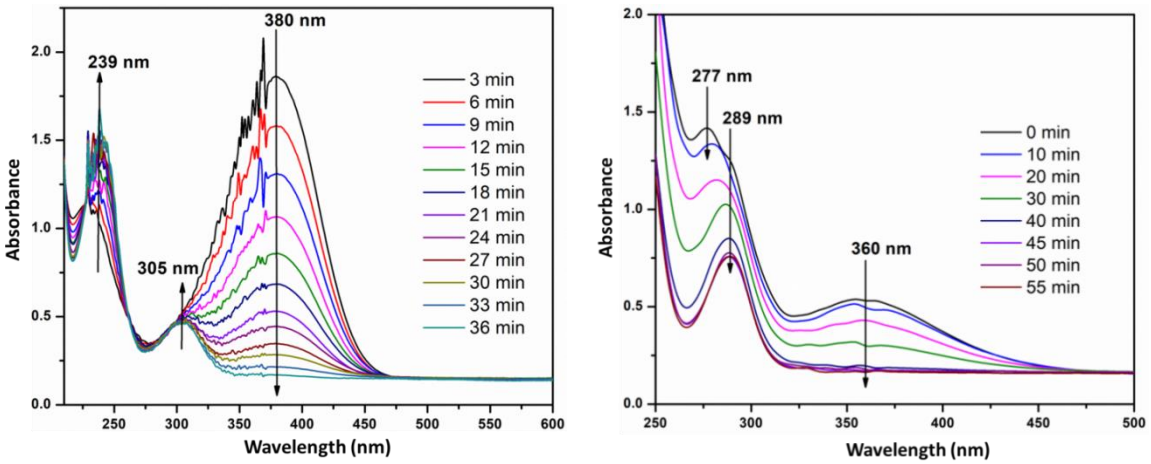

(a) (b)

Figure 3.12 UV-visible spectra screening the reduction of *p*-NA (a) and *m*-NA (b) to the corresponding phenylenediamine.

The characteristic depletion in the absorbance of *p*-NA at 380 nm with the subsequent evolution of two characteristic peaks of *p*-PD at 239 nm and 305 nm in the UV-vis spectrum (Figure 3.12a) of the reaction mixture assures the reaction progress in forward direction. Similarly, the characteristic absorbance peaks of *m*-NA appear at wavelengths 360 nm and 277 nm respectively. The absorbance at 277 nm gradually experiences bathochromic shift and a new absorbance at 289 nm responsible for *m*-PD with the subsequent depletion of absorbance at 360 nm confirms the reaction progress (Figure 3.12b).

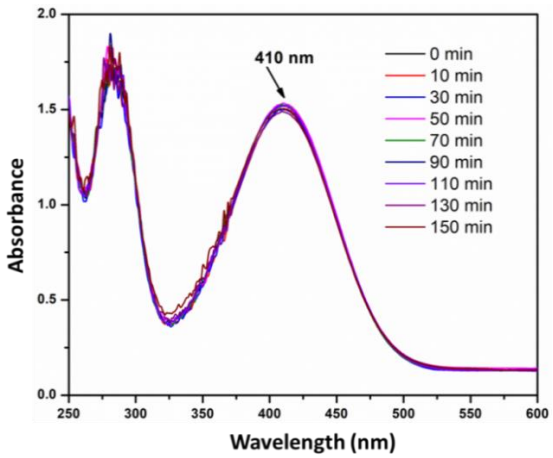

Figure 3.13 UV-vis spectra of reaction mixture of *m*-NA displaying no progress in its reduction.

The planar *o*-NA has better propensity to get adsorbed onto the support matrix *via* π···π interactions as well as intermolecular hydrogen bonding between amino···catalyst *via*

N−H···O=$C_{catalyst}$ and nitro···catalyst *via* N−O···H−$N_{catalyst}$). Thus *ortho* substituted NA shows lesser activity towards the hydride ion to react to yield the reduced product. While NA reduces at considerably faster rate, the *p*-methoxy nitroarene (*p*-MNA) gets reduce at much slower rate. This could be due to the suitable orientation of lone pair electrons in –NH_2 group nitrogen to stabilize the reaction intermediate and a better adsorption property onto the support matrix *via* weak intermolecular interactions. As such the transfer of electrons remains sluggish affecting the reaction rate.

3.3.5 Catalytic reusability of Cu@POP-Am1

Since reusability of catalyst is an important parameter in the heterogeneous catalysis reaction the reusability test of Cu@POP-Am1 in reduction of 4NP to 4AP under identical conditions (as in Figure 3.10) has been performed. After completion of reaction the catalyst was recovered by filtration, repeatedly washed with water, dried at desiccator and reused. Negligible decrease in the catalytic activity of Cu@POP-Am1 has been observed upto the 4th catalytic cycle. The efficiency of catalyst decreases thereafter as it takes almost 1 h for fifth cycle (Figure 3.14) to reduce 4NP. Leaching of Cu to reaction media during reaction progress can't be overlooked. Perhaps the AAS analysis of the reaction filtrate was performed and detected hardly any Cu present in the solution.

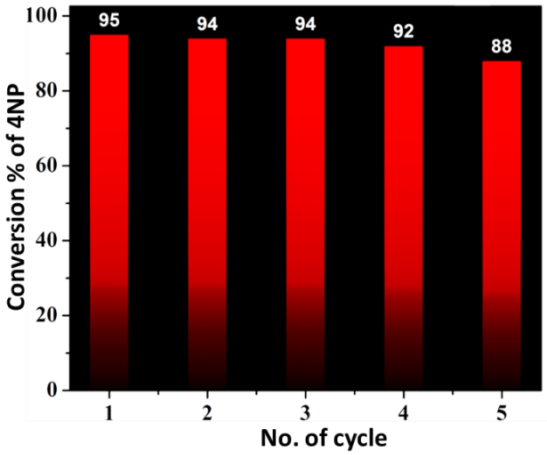

Figure 3.14 Displaying the conversion % of reduction of 4-nitrophenol to 4-aminophenol at each catalytic cycle.

The change in oxidation state of Cu in the reused Cu@POP-Am1 could not be overturned as the catalyst is reduced during the process of reduction reaction. Thus, X-ray photoelectron spectroscopy (XPS) study of reused Cu@POP-Am1 has been conducted (Figure 3.15). The Cu 2p XPS spectrum of Cu@POP-Am1 displays three

bands at 934.09, 943.50 and 954.06 eV. The bands at 934.09 and 954.06 eV attribute the binding energy of Cu $2p_{3/2}$ and Cu $2p_{1/2}$. Whereas, the band at 943.50 eV is responsible to the satellite peak of Cu $2p_{3/2}$. Identical XPS spectrum for Cu(II) immobilized on porous material has also been reported [38]. This signifies that the oxidation state of Cu in reused Cu@POP-Am1 remains unaffected.

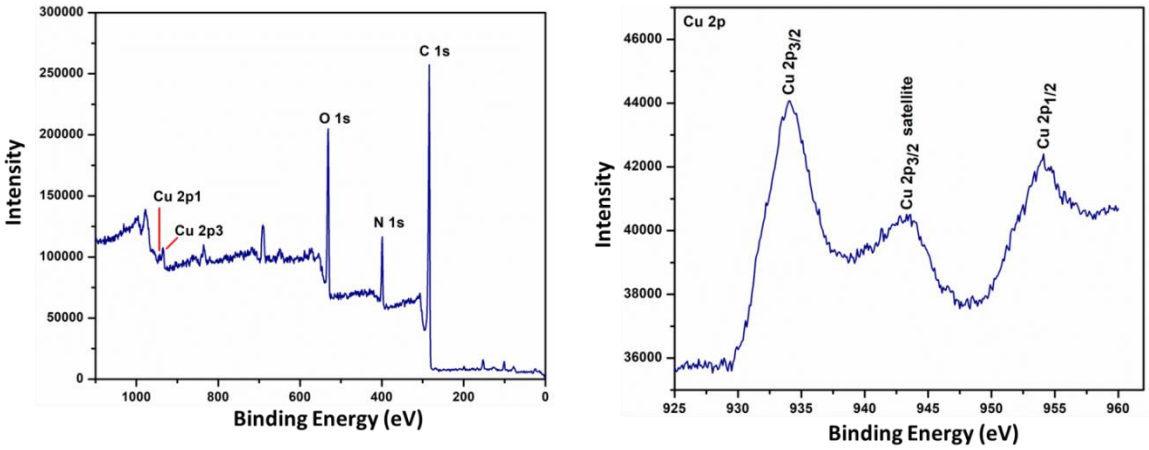

(a) (b)

Figure 3.15 XPS spectrum of (a) Cu@POP-Am1 and (b) Cu 2p of Cu@POP-Am1 revealing the presence of Cu in +2 oxidation state.

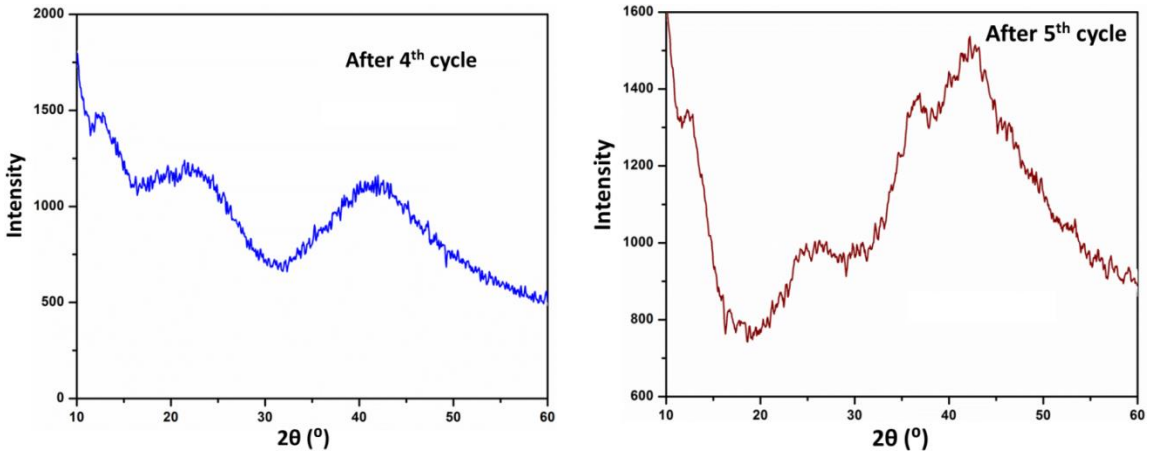

(a) (b)

Figure 3.16 PXRD pattern of reused Cu@POP-Am1 clearly displays the structural integrity degradation of Cu loaded POP-Am1 after 5th catalytic cycle.

Furthermore the stability of reused Cu@POP-Am1 was assured by recording its PXRD pattern (Figure 3.16). The recorded pattern after 4th cycle discloses the identical stability and structural integrity of Cu@POP-Am1 with some change in peak intensity. But the pattern recorded after 5th cycle indicates the deterioration of the structural integrity of

Cu@POP-Am1. Possibly, due to this change in structure the efficacy and effectivity of Cu@POP-Am1 is poisoned and eventually the completion and reaction time gets affected.

3.3.6 Reaction mechanism study of 4NP reduction

A close observation on the catalytic reduction cycle of 4NP with $NaBH_4$ describes the electron transfer rate between the BH_4^- donor and the respective acceptor molecules. The Cu@POP-Am1 plays a pivotal role by acting as intercessor for electron transfer. In order to understand the role of Cu(II) onto the support matrix, another set of reaction with bare POP-Am1 has been conducted but the reaction did not proceed. Thus the support matrix i.e. porous organic polymer with continuous π-electrons and suitable functionality would play crucial role for electron transfer.

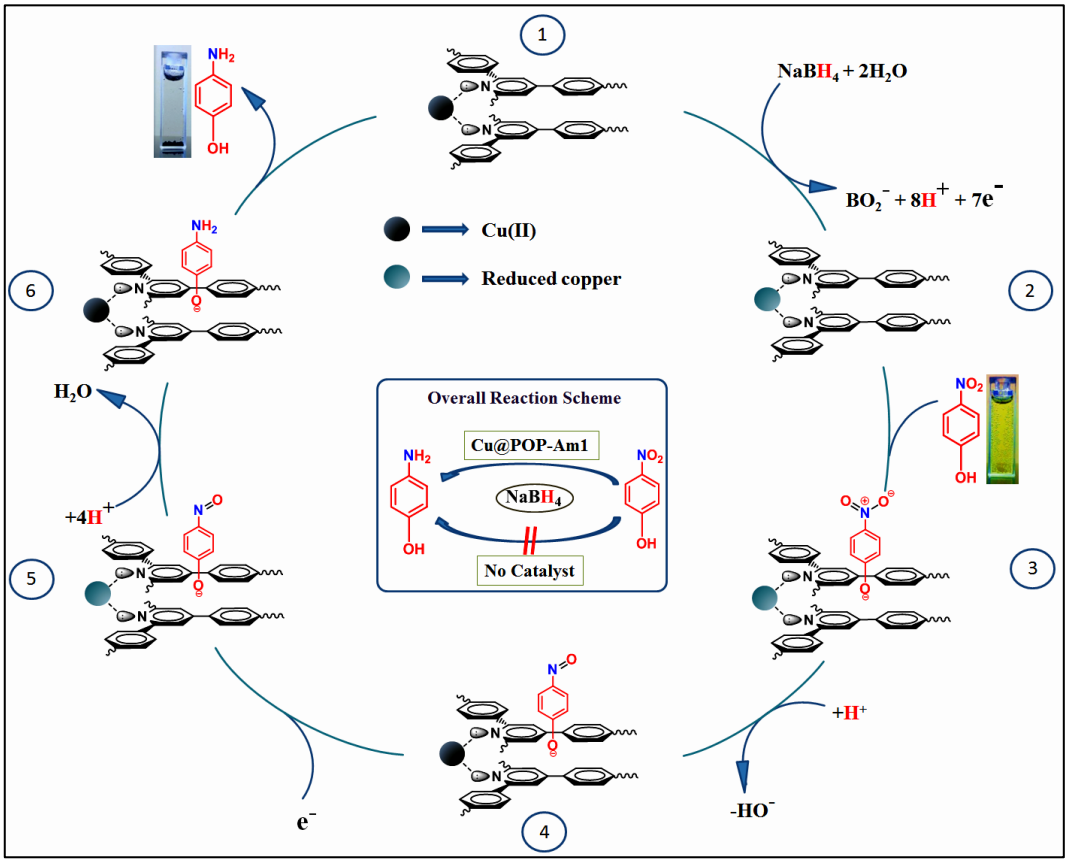

Scheme 3.3 Plausible mechanistic pathway towards reduction of 4-nitrophenol to 4-aminophenol.

Moreover POPs with engineered pores and surfaces provide desirable intermolecular interactions such as hydrogen bonding, ion-dipole interactions, π···π stacking, etc. by

freezing the dynamic nature of nitroarenes and facilitate an appease transfer of electrons. The randomness of phenoxide ion formed initially in the solution adsorbed onto the catalyst surface *via* ion-dipole interaction. Subsequently the electron transfer rate between the BH_4^- donor and the respective acceptor molecule of 4-nitro phenoxide ion improves. The addition of $NaBH_4$ acts not only as hydrogenating agent, but it also reduces Cu(II) to its metastable and/or unstable state in-situ. In the reaction, this reduced copper provides requisite electrons to 4-nitrophenolate and gets oxidize to stable Cu(II) species. The hydrogenating agent $NaBH_4$ then provide the proton against the electron rich 4-nitrophenolate species that is stabilized at the catalyst surface and convert to 4AP eliminating water molecule. The complete catalytic cycle for conversion of 4NP to 4AP is depicted in Scheme 3.3.

3.4 Summary

In this chapter, a pyridine based POP serving as catalytic scaffold for immobilization of cheaper metal, Cu(II) with improved catalytic activity towards heterogeneous reduction of nitroarene is illustrated. Metal incorporation onto the surface/pores of POP-Am1 propagates the higher number of active centers across the organic polymer thereby fastening the reaction kinetics. Noteworthy to mention that reduction of a toxic water pollutant like 4-NP to environmentally benign and biologically important molecule, 4-AP within 90 sec heterogeneously by Cu(II) is an overwhelming outcome. The highly dispersed Cu in Cu@POP-Am1 acts as an agent in propagating the necessary electrons from the porous polymer for performing the reduction reaction smoothly. High stability, no metal leaching and recoverable by only simple filtration after the reaction completion is notable advantages. Therefore present study contributes an alternate and effective route of using a catalytic polymer bed loaded with cheaper metals in various organic reactions.

3.5 Experimental Section

3.5.1 Materials

1,3,5-Benzenetricarbonyl trichloride and 1,4-dioxane (HPLC grade) were purchased from Alfa Aesar and Rankem. The 4-nitrobenzaldehyde and 4-nitroacetophenone have been obtained from Himedia. Ammonium acetate, glacial acetic acid, ethanol and hydrazine monohydrate were purchased from Merck. Activated palladium charcoal was

purchased from Sigma Aldrich. All the chemicals used in the synthetic procedure were used as obtained without further purification.

3.5.2 Synthesis of POP-Am1 and Cu@POP-Am1

3.5.2.1 Synthesis of 2,4,6-Tris(4-aminophenyl)pyridine (TAPPy)

2,4,6-Tris(4-aminophenyl)pyridine (TAPPy) was synthesized following the reported procedure [46]. The 4-nitrobenzaldehyde (50 mg, 0.33 mmol), 4-nitroacetophenone (109 mg, 0.66 mmol) and ammonium acetate (38 mg, 0.5 mmol) were taken in a round bottom flask and added 1 mL glacial acetic acid. The mixture was refluxed for 6 h. Reddish brown precipitate of 2,4,6-tris(4-nitrophenyl)pyridine (TNPP) was obtained on cooling the mixture. The precipitate was filtered, washed with acetic acid and cooled ethanol mixture and then dried under vacuum. TNPP thus prepared was placed in 50 mL round bottom flask containing 5 mL of dry ethanol and heated at 80 °C. To the reaction mixture added 30 mg palladium on activated charcoal (Pd 10%) and excess of hydrazine monohydrate drop wise. The reaction mixture was allowed to reflux for 8 h at 80 °C. Filtered the reaction mixture while hot and washed with hot ethanol. The filtrate was evaporated to yield the yellow solid of desired TAPPy and characterized by NMR spectroscopy.

3.5.2.2 Synthesis of POP-Am1

Dissolve TAPPy (352 mg) in 20 mL dry 1,4-dioxane and pour in 100 mL round bottom flask and added 2 mL of triethylamine (TEA) to the solution. To the mixture dioxane solution (3 mL) of 1,3,5-benzenetricarbonyl trichloride (BzCl, 265.6 mg) was added drop wise and left stirring for 12 h under inert atmosphere (Scheme 3.1). The light yellow precipitate of desired POP-Am1 was allowed to settle down, decanted and purified *via* washing with acetone for five times.

3.5.2.3 Synthesis of copper loaded POP-Am1 (Cu@POP-Am1)

A mixture of POP-Am1 (50 mg) and copper acetate monohydrate (5 mg) in 5 mL dichloromethane (DCM) was stirred for 24 h at room temperature. The reaction mixture was filtered, washed the solid with DCM, methanol, water and acetone to remove the non-adsorbed copper acetate. The obtained solid of Cu@POP-Am1 was dried under vacuum desiccator to ensure solvent free material. The amount of copper loaded was determined using EDS, AAS and ICP analysis.

3.5.3 Characterization/Instrumentation

3.5.3.1 FT-IR spectroscopy

FT-IR spectra were recorded in the frequency range of 400–4000 cm^{-1} in Perkin Elmer spectrophotometer. Approximately 1 mg of the sample to be recorded was ground with 100 mg of dry KBr and pressed the mixture by hydraulic pressure to afford the suitable pellet for recording the IR spectrum.

3.5.3.2 X–ray powder diffraction (PXRD)

PXRD patterns were recorded on Bruker AXS (D8 FOCUS) using Cu Kα radiation with 2θ ranging from 10°– 60° (step size 0.01°) at the rate of 1° min^{-1}. A sample of 50 mg vacuum dried (for 1 h) ground fine powder was taken and recorded PXRD.

3.5.3.3 Solid state NMR (ssNMR)

Solid state ^{13}C cross polarizing magic angle spinning (^{13}C CP-MAS) NMR data was recorded in Jeol 400 MHz spectrophotometer with spin rate of 5000 Hz employing 4 nm MAS probe. Nearly 400 mg of vacuum dried ground fine powder was taken and recorded ssNMR.

3.5.3.4 Thermogravimetric analysis (TGA)

10 mg of dried sample was taken for TGA analysis and recorded the thermogram at Schimadzu thermal analyzer under constant flow of nitrogen at heating rate of 10 °C min^{-1}.

3.5.3.5 BET surface area analysis

The porosity and rigidity of the material was recorded in Brunauer– Emmett–Teller (BET) surface area analyzer (NOVA-1000 Ver 3.70). Before measuring the N_2 adsorption-desorption isotherm and surface area, the material was degassed at 200 °C for 4 h. The analysis was performed using ultra high purity nitrogen (99.999% pure), while the temperature during the process was assured by refrigerated bath of liquid nitrogen (77K).

3.5.3.6 Electron microscopy

SEM images and electron dispersive X-ray spectrophotometer (EDS) were recorded using scanning electron microscopy (SEM, JEOL JSM 6390) at the accelerating voltage

of 200 kV. TEM images of the material dispersed at methanol were collected in JEOL (JEM-2100) at operating voltage of 200 kV.

3.5.3.7 UV spectroscopy

UV–vis spectroscopy has been employed to monitor the progress of the catalytic reaction. In the process, placed 3 mL of the reaction mixture in the Quartz cuvette and recorded the UV-spectrum at the wavelength ranging from 200 to 600 nm in Agilent Cary 60 spectrophotometer.

3.5.3.8 Atomic analysis

Transition metal analysis was performed using atomic absorption spectrophotometer (AAS, Perkin Elmer–3110) and Inductively Coupled Plasma (ICP, Perkin Elmer Optima 2100DV) techniques. In the process, dissolved 100 mg of Cu loaded POP-Am1 in concentrated nitric acid solution, retrieved 1 mL of the mixture and diluted to 100 mL. The dilute solution was further filtered and considered for performing AAS and ICP analysis to calculate the quantitative amount of Cu loaded in POP-Am1.

3.6 References

[1] Aditya, T., Pal, A. and Pal, T. Nitroarene reduction: a trusted model reaction to test nanoparticle catalysts. *Chemical Communications*, 51(46):9410-9431, 2015.

[2] Tang, D., Sun, X., Zhao, D., Zhu, J., Zhang, W., Xu, X. and Zhao, Z. Nitrogen-doped carbon xerogels supporting palladium nanoparticles for selective hydrogenation reactions: The role of pyridine nitrogen species. *ChemCatChem*, 10(6):1291-1299, 2018.

[3] Deka, P., Sarmah, P., Deka, R. C. and Bharali, P. Hetero-nanostructured Ni/α-Mn_2O_3 as highly active catalyst for aqueous phase reduction reactions. *ChemistrySelect*, 1(15):4726-4735, 2016.

[4] Cui, X., Long, Y., Zhou, X., Yu, G., Yang, J., Yuan, M., Ma, J. and Dong, Z. Pd-doped Ni nanoparticle-modified N-doped carbon nanocatalyst with high Pd atom utilization for the transfer hydrogenation of nitroarenes. *Green Chemistry*, 20(5):1121-1130, 2018.

[5] Kim, E., Jeong, H. S. and Kim, B. M. Efficient chemoselective reduction of nitro compounds and olefins using Pd–Pt bimetallic nanoparticles on functionalized multi-wall-carbon nanotubes. *Catalysis Communications*, 45:25-29, 2014.

[6] Dhar, J. and Patil, S. Self-assembly and catalytic activity of metal nanoparticles immobilized in polymer membrane prepared via layer-by-layer approach. *ACS Applied Materials & Interfaces*, 4(3):1803-1812, 2012.

[7] Jiang, H. L., Akita, T., Ishida, T., Haruta, M. and Xu, Q. Synergistic catalysis of Au@Ag core−shell nanoparticles stabilized on metal-organic framework. *Journal of the American Chemical Society*, 133(5):1304-1306, 2011.

[8] Lee, H., Kim, H., Choi, T. J., Park, H. W. and Chang, J. Y. Preparation of a microporous organic polymer by the thiol-yne addition reaction and formation of Au nanoparticles inside the polymer. *Chemical Communications*, 51(48):9805-9808, 2015.

[9] Cao, H. L., Huang, H. B., Chen, Z., Karadeniz, B., Lü, J. and Cao, R. Ultrafine silver nanoparticles supported on a conjugated microporous polymer as high-performance nanocatalysts for nitrophenol reduction. *ACS Applied Materials & Interfaces*, 9(6):5231-5236, 2017.

[10] Luo, P., Xu, K., Zhang, R., Huang, L., Wang, J., Xing, W. and Huang, J. Highly efficient and selective reduction of nitroarenes with hydrazine over supported rhodium nanoparticles. *Catalysis Science & Technology*, 2(2):301-304, 2012.

[11] Veerakumar, P., Madhu, R., Chen, S. M., Veeramani, V., Hung, C. T., Tang, P. H., Wang, C. B. and Liu, S. B. Highly stable and active palladium nanoparticles supported on porous carbon for practical catalytic applications. *Journal of Materials Chemistry A*, 2(38):16015-16022, 2014.

[12] Min, J., Wang, F., Cai, Y., Liang, S., Zhang, Z. and Jiang, X. Azeotropic distillation assisted fabrication of silver nanocages and their catalytic property for reduction of 4-nitrophenol. *Chemical Communications*, 51(4):761-764, 2014.

[13] Pachfule, P., Kandambeth, S., Díaz, D. D. and Banerjee, R. Highly stable covalent organic framework–Au nanoparticles hybrids for enhanced activity for nitrophenol reduction. *Chemical Communications*, 50(24):3169-3172, 2014.

[14] Xie, K., He, Y., Zhao, Q., Shang, J., Gu, Q., Qiao, G. G. and Webley, P. A. Pd(0) loaded $Zn_2(azoBDC)_2(dabco)$ as a heterogeneous catalyst. *CrystEngComm*, 19(29):4182-4186, 2017.

[15] Li, M., Xu, F., Li, H. and Wang, Y. Nitrogen-doped porous carbon materials: promising catalysts or catalyst supports for heterogeneous hydrogenation and oxidation. *Catalysis Science & Technology*, 6(11):3670-3693, 2016.

[16] Pei, Z., Li, H., Huang, Y., Xue, Q., Huang, Y., Zhu, M., Wang, Z. and Zhi, C. Texturing in situ: N, S-enriched hierarchically porous carbon as a highly active reversible oxygen electrocatalyst. *Energy & Environmental Science*, 10(3):742-749, 2017.

[17] Patel, M. A., Luo, F., Khoshi, M. R., Rabie, E., Zhang, Q., Flach, C. R., Mendelsohn, R., Garfunkel, E., Szostak, M. and He, H. P-Doped porous carbon as metal free catalysts for selective aerobic oxidation with an unexpected mechanism. *ACS Nano*, 10(2):2305-2315, 2016.

[18] Long, J., Xie, X., Xu, J., Gu, Q., Chen, L. and Wang, X. Nitrogen-doped graphene nanosheets as metal-free catalysts for aerobic selective oxidation of benzylic alcohols. *ACS Catalysis*, 2(4):622-631, 2012.

[19] Sun, W., Meng, Y., Fu, Q., Wang, F., Wang, G., Gao, W., Huang, X. and Lu, F. High-yield production of boron nitride nanosheets and its uses as a catalyst support for hydrogenation of nitroaromatics. *ACS Applied Materials & Interfaces*, 8(15):9881-9888, 2016.

[20] Singuru, R., Dhanalaxmi, K., Shit, S. C., Reddy, B. M. and Mondal, J. Palladium nanoparticles encaged in a nitrogen-rich porous organic polymer: constructing a promising robust nanoarchitecture for catalytic biofuel upgrading. *ChemCatChem*, 9(13):2550-2564, 2017.

[21] Mondal, S., Singuru, R., Chandra Shit, S., Hayashi, T., Irle, S., Hijikata, Y., Mondal, J. and Bhaumik, A. Ruthenium nanoparticle-decorated porous organic network for direct hydrodeoxygenation of long-chain fatty acids to alkanes. *ACS Sustainable Chemistry & Engineering*. 6(2):1610-1619, 2018.

[22] Dhanalaxmi, K., Singuru, R., Mondal, S., Bai, L., Reddy, B. M., Bhaumik, A. and Mondal, J. Magnetic nanohybrid decorated porous organic polymer: synergistic catalyst for high performance levulinic acid hydrogenation. *ACS Sustainable Chemistry & Engineering*, 5(1):1033-1045, 2016.

[23] Shit, S. C., Khilari, S., Mondal, I., Pradhan, D. and Mondal, J. The design of a new cobalt sulfide nanoparticle implanted porous organic polymer nanohybrid as a smart and durable water-splitting photoelectrocatalyst. *Chemistry-A European Journal*, 23(59):14827-14838, 2017.

[24] Kundu, S. K., Singuru, R., Hayashi, T., Hijikata, Y., Irle, S. and Mondal, J. Constructing sulfonic acid functionalized anthracene derived conjugated porous

prganic polymer for efficient metal-free catalytic acetalization of bio-glycerol. *ChemistrySelect*, 2(17):4705-4716, 2017.

[25] Shit, S. C., Singuru, R., Pollastri, S., Joseph, B., Rao, B. S., Lingaiah, N. and Mondal, J. Cu–Pd bimetallic nanoalloy anchored on a N-rich porous organic polymer for high-performance hydrodeoxygenation of biomass-derived vanillin. *Catalysis Science & Technology*. 8:2195-2210, 2018.

[26] Khatioda, R., Talukdar, D., Saikia, B., Bania, K. K. and Sarma, B. Constructing two dimensional amide porous polymer to promote selective oxidation reactions. *Catalysis Science & Technology*, 7(14):3143-3150, 2017.

[27] Holst, J. R., Trewin, A. and Cooper, A. I. Porous organic molecules. *Nature Chemistry*, 2(11):915, 2010.

[28] Tian, J., Thallapally, P. K. and McGrail, B. P. Porous organic molecular materials. *CrystEngComm*, 14(6):1909-1919, 2012.

[29] Lin, S., Diercks, C. S., Zhang, Y. B., Kornienko, N., Nichols, E. M., Zhao, Y., Paris, A. R., Kim, D., Yang, P., Yaghi, O. M. and Chang, C. J. Covalent organic frameworks comprising cobalt porphyrins for catalytic CO_2 reduction in water. *Science*, 349(6253):1208-1213, 2015.

[30] Saha, B., Gupta, D., Abu-Omar, M. M., Modak, A. and Bhaumik, A. Porphyrin-based porous organic polymer-supported iron (III) catalyst for efficient aerobic oxidation of 5-hydroxymethyl-furfural into 2, 5-furandicarboxylic acid. *Journal of Catalysis*, 299:316-320, 2013.

[31] Weston, M. H., Farha, O. K., Hauser, B. G., Hupp, J. T. and Nguyen, S. T. Synthesis and metalation of catechol-functionalized porous organic polymers. *Chemistry of Materials*, 24(7):1292-1296, 2012.

[32] Fang, H., Sun, S., Liao, P., Hu, Y. and Zhang, J. Gold nanoparticles confined in imidazolium-based porous organic polymers to assemble a microfluidic reactor: controllable growth and enhanced catalytic activity. *Journal of Materials Chemistry A*, 6(5):2115-2121, 2018.

[33] Ding, S. Y., Gao, J., Wang, Q., Zhang, Y., Song, W. G., Su, C. Y. and Wang, W. Construction of covalent organic framework for catalysis: Pd/COF-LZU1 in Suzuki–Miyaura coupling reaction. *Journal of the American Chemical Society*, 133(49):19816-19822, 2011.

[34] Puthiaraj, P. and Pitchumani, K. Triazine-based mesoporous covalent imine polymers as solid supports for copper-mediated Chan–Lam cross-coupling N-arylation reactions. *Chemistry-A European Journal*, 20(28):8761-8770, 2014.

[35] Fang, Q., Gu, S., Zheng, J., Zhuang, Z., Qiu, S. and Yan, Y. 3D Microporous base-functionalized covalent organic frameworks for size-selective catalysis. *Angewandte Chemie International Edition*, 53(11):2878-2882, 2014.

[36] Li, H., Pan, Q., Ma, Y., Guan, X., Xue, M., Fang, Q., Yan, Y., Valtchev, V. and Qiu, S. Three-dimensional covalent organic frameworks with dual linkages for bifunctional cascade catalysis. *Journal of the American Chemical Society*, 138(44):14783-14788, 2016.

[37] Bi, Q. Y., Lin, J. D., Liu, Y. M., He, H. Y., Huang, F. Q. and Cao, Y. Dehydrogenation of formic acid at room temperature: Boosting palladium nanoparticle efficiency by coupling with pyridinic-nitrogen-doped carbon. *Angewandte Chemie International Edition*, 55(39):11849-11853, 2016.

[38] Mu, M., Wang, Y., Qin, Y., Yan, X., Li, Y. and Chen, L. Two-dimensional imine-linked covalent organic frameworks as a platform for selective oxidation of olefins. *ACS Applied Materials & Interfaces*, 9(27):22856-22863, 2017.

[39] Chan-Thaw, C. E., Villa, A., Katekomol, P., Su, D., Thomas, A. and Prati, L. Covalent triazine framework as catalytic support for liquid phase reaction. *Nano Letters*, 10(2):537-541, 2010.

[40] Puthiaraj, P. and Pitchumani, K. Palladium nanoparticles supported on triazine functionalised mesoporous covalent organic polymers as efficient catalysts for Mizoroki–Heck cross coupling reaction. *Green Chemistry*, 16(9):4223-4233, 2014.

[41] Wu, Y., Xu, H., Chen, X., Gao, J. and Jiang, D. A π-electronic covalent organic framework catalyst: π-walls as catalytic beds for Diels–Alder reactions under ambient conditions. *Chemical Communications*, 51(50):10096-10098, 2015.

[42] Khatioda, R., Pathak, D. and Sarma, B. Cu (II) Complex onto a pyridine-based porous organic polymer as a heterogeneous catalyst for nitroarene reduction. *ChemistrySelect*, 3(23):6309-6320, 2018.

[43] Suresh, V. M., Bonakala, S., Atreya, H. S., Balasubramanian, S. and Maji, T. K. Amide functionalized microporous organic polymer (Am-MOP) for selective CO_2 sorption and catalysis. *ACS Applied Materials & Interfaces*, 6(7):4630-4637, 2014.

[44] Karak, S., Kumar, S., Pachfule, P. and Banerjee, R. Porosity prediction through hydrogen bonding in covalent organic frameworks. *Journal of the American Chemical Society*, 140(15):5138–5145, 2018.

[45] Noh, J. H. and Meijboom, R. Catalytic evaluation of dendrimer-templated Pd nanoparticles in the reduction of 4-nitrophenol using Langmuir–Hinshelwood kinetics. *Applied Surface Science*, 320:400-413, 2014.

[46] Chen, W., Yan, W., Wu, S., Xu, Z., Yeung, K. W. K. and Yi, C. Preparation and properties of novel triphenylpyridine-containing hyperbranched polyimides derived from 2,4,6-tris(4-aminophenyl) pyridine under microwave irradiation. *Macromolecular Chemistry and Physics*, 211(16):1803-1813, 2010.